33rd Annual International Conference of the IEEE EMBS
Boston, Massachusetts USA, August 30 - September 3, 2011

An Improved Algorithm for Quantifying Real-time Impedance Biosensor Signals

Dean S. Messing, *Member, IEEE*, Andrey Ghindilis, and Kevin Schwarzkopf

***Abstract*— In previously published work [1] we presented a real-time electrochemical impedance biosensor prototype system and a state-space estimation algorithm for signal quantification. Experiments in the interim have revealed some algorithm failure modes which reduced the reliability and repeatability of quantification. The present work describes a related algorithm that introduces constraints based on *a priori* knowledge of the expected signals predicted by the biosensor signal model. The improvements in reliability and repeatability bring the system close to deployment for real-world trials.**

***Index Terms*— parameter estimation; signal model; prior knowledge; impedance biosensor signal quantification**

I. INTRODUCTION

Recent advances in unlabeled, electrochemical impedance biosensor technology have made it a viable and enabling tool for the clinical and life-sciences communities. Point-of-care and portable, in-field applications especially stand to benefit from its real-time operation.

Systems using an affinity-based impedance readout detect changes at the sensor surface due to binding between an immobilised layer of *probe* molecules and a sample containing *target* (or *analyte*) molecules to be detected or measured. Binding causes changes in the electrical *double-layer* which are manifested by measurable changes in the circuit impedance of the electrode—double-layer—solution interface.

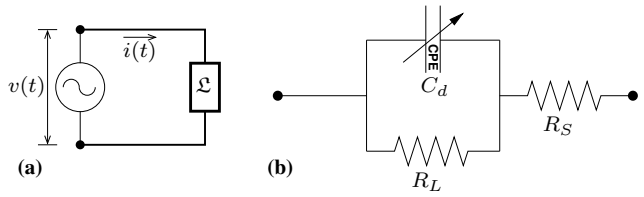

Fig. 1. **(a)**: Impedance measurement configuration **(b)**: Equivalent circuit of surface/solution interface

Most target detection methods use *Electrochemical Impedance Spectroscopy* (EIS) to measure the impedance spectrum of the sensor during a binding event [2].

Fig. 1(a) depicts a typical one-port quasi-linear device, $\mathfrak{L}$, driven by stimulus voltage, $v(t)$, and having response current, $i(t)$. The device, $\mathfrak{L}$, represents the impedance sensor of a biosensor instrument. A commonly assumed equivalent circuit model for the electrode-electrolyte interface in non-faradaic operation—to which this paper is limited—is shown in Fig. 1(b), where R_S is the solution resistance of the electrolyte. This resistance is in series with a parallel connection of R_L, the leakage resistance associated with the double-layer, and C_d, the double-layer capacitance, often modeled by a *constant phase element* (CPE)[1] [3].

The dominant indicator of target binding is a continuous change (until equilibrium) in the value of C_d, suggested by the "variable arrow" through C_d in Fig. 1(b). Estimates of C_d are obtained by using Fig. 1(b) as a model which is fit to the EIS spectra acquired during binding.

Alternate approaches to target detection and measurement differ from EIS in that no circuit model is assumed and no spectra are computed. Instead, the time-varying impedance response at a single frequency is directly used to deduce either the presence of specific target or information about the binding kinetics. *Endpoint methods* measure the absolute change in impedance from analyte injection until binding equilibrium. Results from such methods require long waiting times (40-80 minutes are typical in ssDNA applications). *Real-time methods* use the changing impedance signal as binding proceeds. Quantitative conclusions can thus be quickly drawn early in the binding process. One such real-time detection method is based on the initial response slope [4]. Repeated area integration of the dynamic response has also been suggested. These methods, however, return only a scalar quantity that does not well reflect the kinetic binding information. In [1], we presented a prototype impedance biosensor system that used state-space estimation capable of delivering signal parameters that were tied to the binding kinetics. Further development of the biochemical protocols, the instrumentation, and the algorithm have proceeded in the interim. This paper focuses on the latter.

The algorithmic approach taken in [1] (and here) directly uses the real-time impedance profile at a single frequency. We assume an underlying binding model that is a function of time. Such a model is described, for example, by the well-known *Langmuir Isotherm* which approximates binding in many practical cases. This gives rise to a mathematical *signal model* which the time-dependent biosensor impedance should obey (in the ideal case) as target binding proceeds. The goal of the algorithm is to reliably and repeatably estimate the model parameters. During the course of testing on real-world biosignals, we discovered certain failure modes in

All authors are with Sharp Laboratories of America, 5750 NW Pacific Rim Blvd, Camas, Washington, 98607, USA.
Corresponding author e-mail: deanm@sharplabs.com

[1] A CPE has complex impedance given by $1/((j\omega)^{\alpha}Q)$ where ω is radian frequency, Q is analogous to capacitance, and $0.5 < \alpha < 1.0$ is a parameter that allows for modeling the sub-90° phase shift that is empirically observed at the interface of solid metal electrodes. When $\alpha = 1$ the element behaves like an ordinary capacitor with $Q = C_d$.

978-1-4244-4122-8/11/$26.00 ©2011 IEEE

the estimation that were tied to the large amount of non-linear signal noise, including deviations from the model. This paper describes the improvements made to the estimation procedure. These improvements prevent failures and reduce estimation variance to a level acceptable for external prototype deployment for field testing.

The paper is organised as follows. Section II discusses the biosignal model upon which the estimation algorithm operates. In Section III we discuss the algorithmic failure modes that we discovered as testing on real-world biosignals proceeded. We discuss their cause and propose a constrained estimation procedure that uses *a priori* knowledge of the signal model. Section IV demonstrates the improvements that the constrained algorithm gives in terms of key results presented in [1]. Finally, Section V draws conclusions from the results.

II. BIOSIGNAL MODEL

Assumption of a probe-target binding model as discussed above leads to a signal model that obeys an exponential function whose binding rate decreases with time after analyte is introduced into the buffer solution containing the biosensor.

This function of time, or sample index n in the discrete-time case, is well-modeled by

$$|Z(t)| = A_1 - A_2 e^{-\alpha t} + \nu(t), \tag{1}$$

where $\alpha, A_k \geq 0$ are constants.

Before injection of analyte, $|Z(t)|_{t=0} = A_1 - A_2$ corresponds to the constant offset at which the response starts, and (ignoring drift) represents the biosensor baseline impedance which is dependent on sensor topology, buffer concentration, temperature, and stimulus frequency. The noise inherent in all impedance biosensors is represented by ν. Shown in black

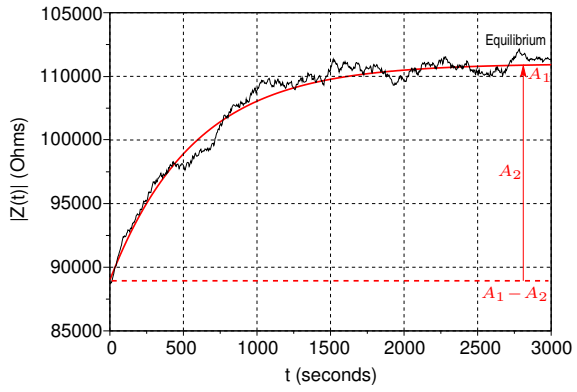

Fig. 2. Typical noisy impedance signal (black) and impedance model function without noise (red).

in Fig. 2 is a typical noisy impedance signal during target binding. An estimation algorithm takes such a signal as input and extracts the exponential time constant, α, exponential amplitude, A_2, and the equilibrium (endpoint) amplitude, A_1. From these an estimate of the underlying model function can be computed from Eq. 1. An example model function is shown by the red curve in Fig. 2.

Both α and A_2 hold important biochemical information. The former tracks analyte concentration, and the latter is a function of sensor surface coverage, which is correlated to molecular affinity. An extended biosignal model, $|Z(t)| = A_1 - \sum_{k=2}^{p} A_k e^{-\alpha_k t} + \nu(t)$, where $\alpha_k, A_k \geq 0$, applies when two or more binding processes occur at once, as is the case with specific and non-specific binding. In either the $p = 2$ or $p > 2$ case, the magnitude(s) of α_k tend to be small and in proximity to the trivial exponential represented by $A_1 = A_1 e^{-\alpha_1 t}|_{\alpha_1=0}$.

The main difficulties in estimating the parameters of either Eq. 1 or the multiple exponential model are the closely spaced *poles* in the complex frequency domain, the substantial additive noise in the impedance signals, and the non-linear involvement of the parameters. To overcome the difficulties, we investigated a number of increasingly advanced deterministic estimation algorithms and settled on the method presented in [5], as discussed in [1].

The method of [5], and the constrained algorithm discussed in Section III-B assume a general signal model composed of uniformly spaced samples of a sum of p *complex* exponentials corrupted by zero-mean Gaussian noise, $\nu(n)$, and observed over a time aperture of N samples. This is described by the formula

$$\begin{aligned} x(n) &= \sum_{k=1}^{p} a_k e^{s_k n} + \nu(n) \\ &= \sum_{k=1}^{p} a_k z_k^n + \nu(n) \quad n = 0, 1, \ldots, N-1. \end{aligned} \tag{2}$$

where the parameters of the model are the complex amplitudes, $\{a_k\}$, and the complex frequencies, $\{s_k\}$. The latter can be written $s_k = -\alpha_k + j2\pi f_k$, with $\{\alpha_k\}$ being the pole damping factors and $\{f_k\}$ are the pole frequencies. The $\{z_k\}$ are the discrete-time poles of the signal.

It is clear that the biosignal model is a special case of Eq. 2, with two or more *real* poles[2] in the complex Z-plane, $z_1 = 1$ and $z_k = e^{-\alpha_k}$, and real-valued amplitudes, $a_k = A_k$.

III. PARAMETER ESTIMATION

The mathematical description of the estimation procedure used in [1] is presented in [5]. The method is an extension of the *Matrix Pencil* algorithm of [6]. The extension estimates the poles of an *implicitly decimated* signal. No signal sample reduction is needed to accomplish the increased pole separation (and hence increased resolution) that unaliased decimation naturally introduces. On the other hand, the algorithm avoids the increased estimation variance that explicit decimation entails. These features were beneficial to our needs due to the proximity of α to the trivial pole in Eq. 1.

A. Failure modes

As testing and verification progressed, some failure modes were observed. An example of this was provided by the acquired impedance signals shown in Fig. 3. The instrument of [1] simultaneously measures an array of 15 biosensors

[2]We assume that the sampling period has been absorbed into the values of $\{\alpha_k\}$.

organised into three 5-sensor chambers. Two of the three chambers were utilised to obtain the data of Fig. 3(top) where all plots are referenced to 0 seconds.

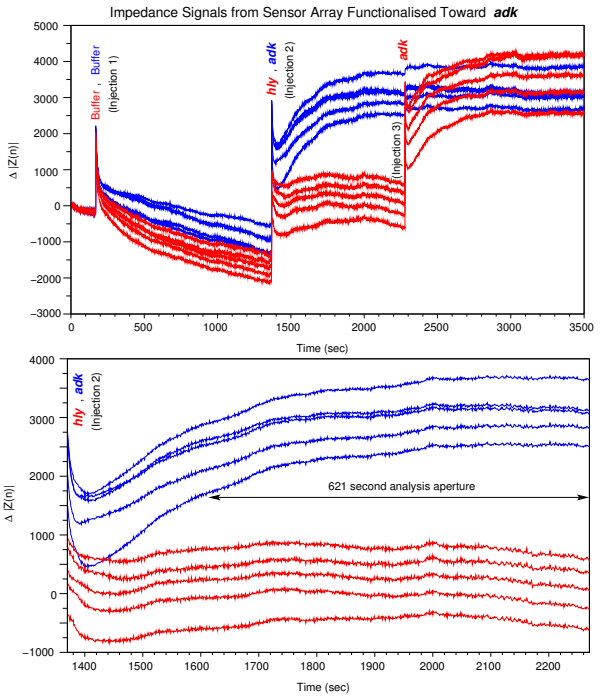

Fig. 3. **Top:** 3600 sec. of impedance data acquired from 10 sensors functionalised toward *adk*. Blue signals show specific response to *adk* target following Injection 2. Red signals show non-specific response of *hly* target injected at the same time. Buffer solution with no analyte was injected at Injection 1 for all sensors. Only drift response is seen. At Injection 3, *adk* was injected in the red channels. Specific response is seen. **Bottom:** Expanded view between Injection 2 and Injection 3. Analysis aperture starts at 1624 sec. and extends to Injection 3.

All sensors were functionalised with probes designed to bind to 35-mer oligonucleotide representing a unique sequence in the adenylate kinase (*adk*) gene of E. coli. In the chamber identified with the blue signals, *adk* target was introduced at Injection 2 and we see the expected noisy exponential *specific response* after an initial transient period. At the same time a negative control analyte, 35-mer oligonucleotide representing a unique sequence in the hemolysin (*hly*) gene of E. coli, was injected into the chamber associated with the red response. We see typical *non-specific* responses from Injection 2 to Injection 3. The specific response data in this segment, expanded in Fig 3(bottom), caused three failure modes.

Fig. 4 depicts in grey the data within the Analysis Aperture of the five specific response channels of Fig 3(bottom). Also shown in red are the five estimated model functions for this data. The data and models for the non-specific channels are not shown but the estimates of α and A_2 are either invalid[3] or the cross-channel statistics indicate variability well outside expected values. Both cases indicate non-specific binding.

We see from at least three of the red model curves in Fig. 4 that something has gone amiss with the estimation

[3]By *invalid* we mean either negative A_k or α_k, or values that are obviously out-of-bounds for normal operation.

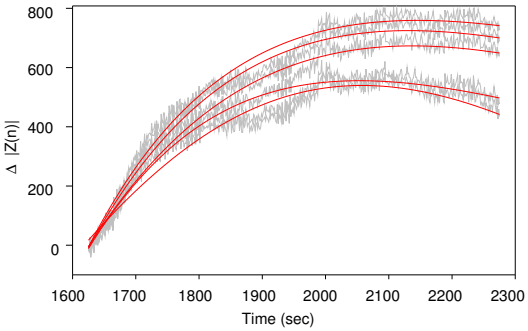

Fig. 4. **grey:** Specific response data within Analysis Aperture of Fig 3(bottom). **red:** Estimated signal model functions for the five responses.

since neither Eq. 1 or its extension for $p > 2$ can give rise to models that decrease. An examination of the estimated signal poles in Fig. 5 reveals three failure modes. For three

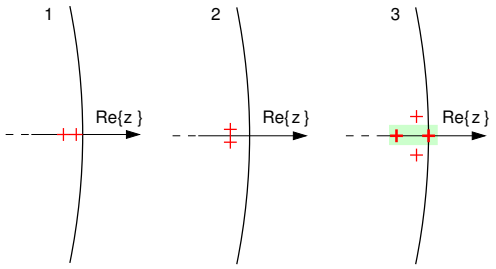

Fig. 5. Signal Pole locations for three failure modes: 1) two negative poles; 2) nearly critically damped; 3) under-damped

of the signals, the estimated poles of Eq. 2 ($p = 2$) have been plotted in the complex z-plane and the region around where the unit circle intersects the $\mathrm{Re}\{z\}$-axis has been expanded.

In the left-hand plot (1), we see that two significant negative poles have been estimated. Neither of the estimated values is close to the expected correct values. The more negative pole underestimates (in absolute value) the expected signal pole by more than 46%. These errors induce even larger errors in the estimates of a_k where, for example, a_2 was estimated to be about 2000 whereas the expected correct value should be in the range 550–800. Since neither pole is constrained in the algorithm of [1], we should expect some small non-zero error in the trivial pole on the unit circle. But in this case the error is ten times the usual value due to large deviation of the signal from the model and low operating SNR. The middle plot (2) shows a second failure mode, the nearly critically damped case. The estimated poles have become complex conjugate though the negative real parts dominate. The real part is still far from the expected correct value and a_k have also become complex. The right-hand plot (3) shows a third failure: the poles are again complex but the the imaginary parts dominate indicating oscillatory behaviour in the estimated model. Clearly, no valid conclusions can be drawn from these estimates.

We extrapolated the model curves in each of these cases out to 4250 seconds and plotted these in Fig. 6 where the impedance data is again shown in grey, the model curves are shown in red, and the their extrapolations are shown in blue.

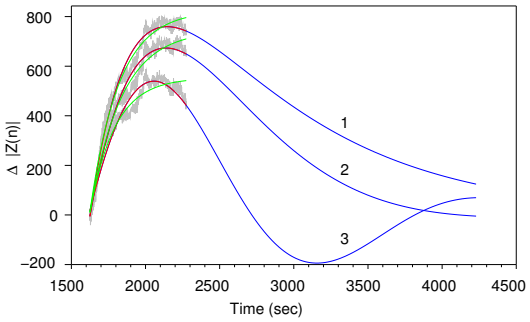

Fig. 6. Extrapolated model curves showing the effect of the three failure modes depicted in Fig. 5. **grey:** Specific response data. **red:** Estimated signal model functions. **blue:** Extrapolated signal model functions. **green:** Constrained signal model functions.

The over-damped, nearly critically damped, and under-damped behaviour is clearly seen in the extrapolated plots. A forth failure mode, not shown, occurs when a substantial drift component (or unexplained electrochemical behaviour) causes an upward-going slope as the response approaches equilibrium. In this case two real poles result but the trivial pole becomes substantially positive, again introducing unacceptably large errors into α and A_2.

In all these cases the problem arose because the known trivial pole was not constrained to $z = 1$. There we investigated constrained algorithms in the same class as the one we used in [1].

B. Constrained Estimation

The estimation algorithms under consideration fall into the class of State-space Signal Modeling approaches that have wide application in signal array processing, medical MR spectrum analysis, speech processing, and now impedance biosignal analysis. The tutorial paper [7] by Rao and Arun contains an excellent discussion of the basic ideas, although much development has occurred since its publication.

All of the state-space algorithms break the general non-linear estimation problem into two steps. The first estimates the $\{z_k\}$ and the second estimates the linearly involved $\{a_k\}$ in Eq. 2, given the poles. Step 1 of all the methods depends on the so-called row or column *shift-invariant* property of the noiseless Hankel matrix formed from $x(n)$ in Eq. 2. Finally all of the techniques involve a principal component, or SVD, decomposition in step 1 to dramatically reduce the effects of noise on the final estimates. The techniques differ by (among other things) when the SVD and the matrix shifting is applied and how decimation is accomplished within the algorithms. Reference [8] discusses the steps of most of the various methods.

We apply the method discussed in [9] and [10] in order to introduce constraints on some pole locations. In brief, this method reduces to writing the noiseless Hankel data matrix, $\mathbf{X}$, of $x(n)$, in terms of its Vandermonde Matrix expansion: $\mathbf{X} = \mathbf{A}\mathbf{C}\mathbf{B}^T$. If m pole locations are known, then m columns of $\mathbf{A}$ may be explicitly specified. We thus form $\mathbf{A}_K$ consisting of the m known columns of $\mathbf{A}$ and then perform a QR decomposition of $\mathbf{A}_K$: $\mathbf{A}_K = \mathbf{Q}\mathbf{R}$. The first m columns of $\mathbf{Q}$ span the column space of $\mathbf{A}_K$, and the remaining columns of $\mathbf{Q}$, $\mathbf{Q}_\perp$, span the orthogonal complement of the column space of $\mathbf{A}_K$. Using $\mathbf{Q}_\perp$ we can thus project $\mathbf{X}$ onto the orthogonal complement of *its* column space, $\hat{\mathbf{X}} = \mathbf{Q}_\perp^H \mathbf{X}$ thus removing the contribution of the known poles from the system. Care must be taken to note that this projection destroys the shift-invariant property of the column space of $\hat{\mathbf{X}}$. However the shift-invariant property of its row space remains intact [11] and may be used to derive a constrained form of the HTLS algorithm[4].

Using the preceding ideas we derived the constrained HTLS algorithm for the case of a known real pole on the unit circle and applied this estimation procedure to our impedance biosensor signals. We note in passing that the constrained algorithm is no longer implicitly decimative. However a number of factors—improvements in (i) the sampling and signal conditioning amplifiers, (ii) sensor array manufacturing process, (iii) sensor surface preparation and bio-functionalisation protocol and, not least of all, the constrained algorithm itself—have removed the need for implicit or explicit decimation so that very small magnitude signal poles can be successfully distinguished from the trivial baseline pole using constrained HTLS alone.

IV. RESULTS

One set of curves, the green model curves in Fig. 6 have not yet been discussed. These curves are the result of applying the constrained algorithm to the biosensor impedance signals in grey. As can be seen the top two green curves have an almost identical decay constants, α. Only the amplitudes, A_2, differ. The bottom curve has a slightly larger (in magnitude) decay constant and a smaller amplitude. In fact, the values of α for all five specific responses in Fig. 4, which include the three under discussion, are within 15% of their average value, and four of them are within 7%—an excellent result given the deformed and noisy character of the signals. The average pole position, and the pole to be on the unit circle are shown in right-hand plot of Fig. 5 in the green-boxed region.

The chief result in [1] was the original algorithm-and-system's ability to statistically distinguish nearby variants or strains of real-world E. coli. In that experiment, ssDNA was used from two E. coli variants, F11 and F24, that differed by just 1 nucleotide in 5. There were four sensors in each of two chambers. All sensors were functionalised toward F11—the the specific target. The difference in affinity to the probe due to the nucleotide variation induced a statistically significant change in A_2 which we detected. The details of the experiment are discussed in [1].

The salient point is that, although we had distinguished the strains, the 95% confidence intervals are only just separated, as can be seen in Fig. 7. Furthermore we could draw no conclusions at the time from the values of α across the array. We assumed that α should have been roughly constant

[4]The basic HTLS algorithm is also known in the literature as TLS-ESPRIT

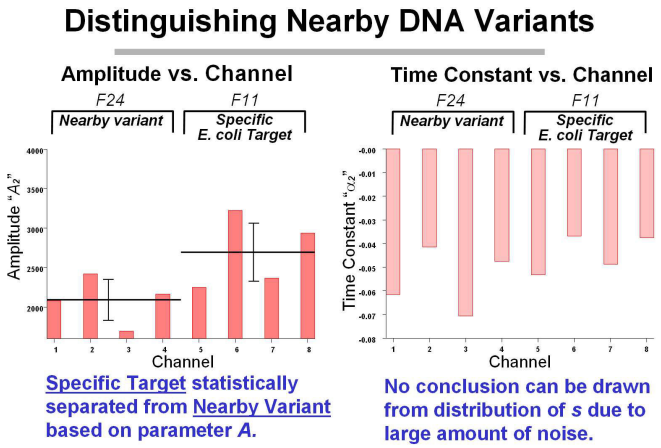

Fig. 7. Estimated response amplitude (A_2 in Eq. 1) plotted against channel. Channels 1–4 correspond to F24 ssDNA target in one chamber, and channels 5–8 to F11 ssDNA and a second chamber. A small statistical separation in A_2 can be seen between the chambers.

across all sensors since target concentration was the same for the F11 chamber and the F24 chamber. Another possibility would have been correlation within each chamber and a possibly significant variation between the two chambers (as with A_2) due to slight differences in the amount of target injected in each chamber, i.e., a slight difference in concentration due to manual pippeting. In fact neither of these could be seen. The variability in α was simply too high due to very low signal quality.

We applied the proposed constrained algorithm to the same data and plotted the new results in blue, overlaid onto the previous results. These are shown in Fig. 8.

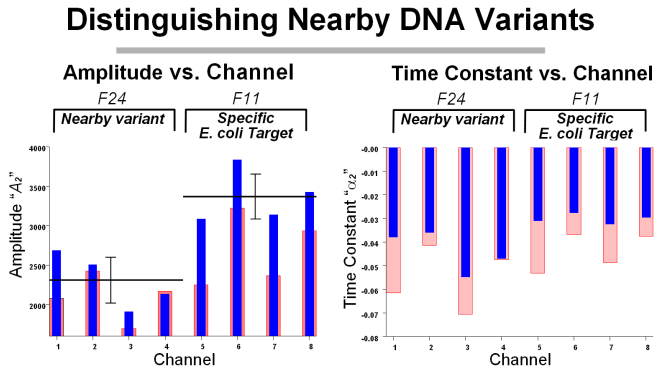

Fig. 8. Bar graphs in blue show the results of applying the constrained estimation scheme to the data of Fig. 7. The statistical separation in A_2 between the chambers is much improved compared to Fig. 7.

As can be easily seen, the statistical separation of the confidence intervals for A_2 is substantially improved. In addition, we can now see the expected behaviour in α. All values in the F11 chamber are slightly smaller in absolute value than those in the F24 chamber. Though this is not important as far as the distinguishing of F11 and F24, which depends only on A_2, it is interesting that the improved algorithm reveals previously invisible details.

V. CONCLUSION

We introduced at EMBC 2010 an impedance biosensor system and state-space signal quantification algorithm for estimating the parameters of acquired biosignals. Extensive testing on real-world DNA affinity binding signals has since revealed various failure modes in the use of that algorithm. The algorithm's key weakness in the context of our biosensor system is the lack of a ready mechanism for introducing constraints based on *a priori* knowledge of the signal model. Here, we have proposed a new constrained algorithm that is appropriate for our signal model. The results are very promising, with no further failure modes observed over a wide variety of difficult analysis cases given by our biochemists, and with a substantial reduction in parameter variance. These results bring the instrument to the point where deployment for external trials can begin. Deployment is, indeed, now only a few weeks away.

REFERENCES

[1] Dean S. Messing, Andrey Ghindilis, and Kevin Schwarzkopf, "Impedimetric biosignal analysis and quantification in a real-time biosensor system," in *Proc. 32nd Int'l. Conf. of the IEEE EMBS*, Buenos Aires, Sept. 2010, pp. 2730–2734.

[2] Byoung-Yong Chang and Su-Moon Park, "Electrochemical impedance spectroscopy," *Annu. Rev. Analytical Chemistry*, vol. 3, pp. 207–229, 2010.

[3] Jonathan S. Daniels and Nader Pourmand, "Label-free impedance biosensors: Opportunities and challenges," *Electroanalysis*, vol. 19, no. 12, pp. 1239–1257, May 2007.

[4] Andrei L. Ghindilis, Maria W. Smith, Kevin R. Schwarzkopf, Changqing Zhan, David R. Evans, António M. Baptista, and Holly M. Simon, "Sensor array: Impedimetric label-free sensing of dna hybridization in real time for rapid, pcr-based detection of microorganisms," *Electroanalysis*, vol. 21, no. 13, pp. 1459–1468, Apr. 2009.

[5] Stavroula-Evita Fotinea, Ioannis Dologlou, and George Carayannis, "On the use of decimation for efficient spectral estimation," *Int'l. J. Computer Maths. & Appl. (HERMIS-μπ)*, vol. 8, pp. 84–100, Oct. 2006.

[6] Y. Hua and T. K. Sarkar, "Matrix pencil method for estimating parameters of exponentially damped/undamped sinusoids in noise," *IEEE Trans. Acous. Speech, Sig. Proc.*, vol. 38, no. 5, pp. 814–824, May 1990.

[7] Bhaskar D. Rao and K. S. Arun, "Model based processing of signals: A state space approach," *Proceedings of the IEEE*, vol. 80, no. 2, pp. 283–309, Feb. 1992.

[8] Geert Morren, Philippe Lemmerling, and Sabine Van Huffel, "Decimative subspace-based parameter estimation techniques," *Sig. Proc.*, vol. 83, pp. 1025–1033, May 2003.

[9] Petre Stoica, Yngve Selén, Niclas Sandgren, and Sabine Van Huffel, "Using prior knowledge in SVD-based parameter estimation for magnetic resonance spectroscopy—the ATP example," *IEEE Trans. Biomed. Eng.*, vol. 51, no. 9, pp. 1568–78, 2004.

[10] Hua Chen, Sabine Van Huffel, and Joos Vandewalle, "Improved methods for exponential parameter estimation in the presence of known pols and noise," *IEEE Trans. Sig. Proc.*, vol. 45, pp. 1390–1393, May 1997.

[11] Hua Chen, Sabine Van Huffel, Ad van den Boom, and Paul van den Bosch, "Subspace-based parameter estimation of exponentially damped sinusoids using prior knowledge of frequency and phase," *Sig. Proc.*, vol. 59, pp. 129–136, May 1997.